

SMOS soil moisture retrievals using the land parameter retrieval model: Evaluation over the Murrumbidgee Catchment, southeast Australia



R. van der Schalie^{a,f,*}, R.M. Parinussa^{a,e}, L.J. Renzullo^b, A.I.J.M. van Dijk^{b,c}, C.-H. Su^d, R.A.M. de Jeu^{a,f}

^a Faculty of Earth and Life Sciences, VU University Amsterdam, Amsterdam, Netherlands

^b CSIRO Land and Water, Canberra, ACT, Australia

^c Fenner School of Environment & Society, The Australian National University, Canberra, ACT, Australia

^d Department of Infrastructure Engineering, University of Melbourne, Victoria, Australia

^e Water Research Centre, University of New South Wales, Sydney, New South Wales, Australia

^f Transmissivity, Noordwijk, Netherlands

ARTICLE INFO

Article history:

Received 23 April 2014

Received in revised form 16 January 2015

Accepted 1 March 2015

Available online 1 April 2015

Keywords:

Remote sensing

Passive microwave radiometry

Soil moisture

Soil Moisture and Ocean Salinity (SMOS)

Land parameter retrieval model (LPRM)

ABSTRACT

The land parameter retrieval model (LPRM) is a methodology that retrieves soil moisture from low frequency dual polarized microwave measurements and has been extensively tested on C-, X- and Ku-band frequencies. Its performance on L-band is tested here by using observations from the Soil Moisture and Ocean Salinity (SMOS) satellite. These observations have potential advantages compared to higher frequencies: a low sensitivity to cloud and vegetation contamination, an increased thermal sampling depth and a greater sensitivity to soil moisture fluctuations. These features make it desirable to add SMOS-derived soil moisture retrievals to the existing European Space Agency (ESA) long-term climatological soil moisture data record, to be harmonized with other passive microwave soil moisture estimates from the LPRM. For multi-channel observations, LPRM infers the effective soil temperature (T_{eff}) from higher frequency channels. This is not possible for a single channel mission like SMOS and therefore two alternative sources for T_{eff} were tested: (1) MERRA-Land and (2) ECMWF numerical weather prediction systems, respectively. SMOS measures brightness temperature at a range of incidence angles, different incidence angle bins (45° , 52.5° and 60°) were tested for both ascending and descending swaths. Three LPRM algorithm parameters were optimized to match remotely sensed soil moisture with ground based observations: the single scattering albedo, roughness and polarization mixing factor. The soil moisture retrievals were optimized and evaluated against ground-based data from the Murrumbidgee Soil Moisture Monitoring Network (OzNet) in southeast Australia. The agreement with single-angle SMOS LPRM retrievals was close to the official SMOS L3 product, provided the three parameters were optimized for the OzNet dataset, with linear correlation of 0.70–0.75 (0.75–0.77 for SMOS L3), root-mean-square error of 0.069–0.085 $\text{m}^3 \text{m}^{-3}$ (0.084–0.106 $\text{m}^3 \text{m}^{-3}$ for SMOS L3) and small bias of -0.02 – $0.01 \text{m}^3 \text{m}^{-3}$ (0.03–0.06 $\text{m}^3 \text{m}^{-3}$ for SMOS L3). These results suggest that the LPRM can be applied successfully to single-angle SMOS L-band observations, but further testing is required to determine if the same set of parameters can be used in other geographic areas.

© 2015 Elsevier Inc. All rights reserved.

1. Introduction

A better understanding of the dynamics of near-surface soil moisture (θ , $\text{m}^3 \text{m}^{-3}$ for a top soil layer of defined thickness) with increased spatial and temporal details can be expected to improve the knowledge of energy and water fluxes between the Earth surface and the atmosphere. Evidence suggests that several important practical applications can benefit from satellite-derived θ estimates, including flood forecasting, drought monitoring and weather and climate modeling (Bisselink,

Van Meijgaard, Dolman, & De Jeu, 2011; Bolten, Crow, Zhan, Jackson, & Reynold, 2010; Brocca et al., 2010). Space-borne microwave observations at low frequencies (i.e. L-band, C-band, X-band) have the potential to fulfill this need. Over the years several algorithms have been developed to derive θ from passive microwave observations, resulting in numerous data products developed from 1978 onwards (Owe, De Jeu, & Holmes, 2008, and references therein). The datasets have proven their value in research applications (e.g., Jung et al., 2010; Liu, De Jeu, Van Dijk, and Owe, 2007; Taylor, De Jeu, Guichard, Harris, & Dorigo, 2012). They become even more valuable once estimates from subsequent satellite missions are combined into one consistent multi-decadal data record (De Jeu et al., 2012). This was addressed by the European Space Agency (ESA) through the Water Cycle MultiMission Observation Strategy (WACMOS) project and the Climate Change Initiative Program

* Corresponding author at: Earth and Climate Cluster, Department of Earth Sciences, Faculty of Earth and Life Sciences, VU University Amsterdam, Amsterdam, The Netherlands, Telephone: +31 (0)20 5983687

E-mail address: r.vander.schalie@vu.nl (R. van der Schalie).

(CCI), in which a single consistent 32 year data record was produced by harmonizing soil moisture estimates from historical passive- and active microwave and observations (Liu et al., 2012a). This data record makes use of the land parameter retrieval model (LPRM) (Owe, De Jeu, & Walker, 2001) to derive soil moisture from the passive microwave sensors and the change detection algorithm to derive θ from the active microwave observations (Wagner, Lemoine, & Rott, 1999) as baseline algorithms to develop the long-term soil moisture record.

The LPRM is one of several methods for inferring θ from passive microwave observations. This method has been applied to observations from multiple passive microwave sensors, such as the Scanning Multi-channel Microwave Radiometer (SMRM), the Special Sensor Microwave Imager (SSM/I), the Tropical Rainfall Measuring Mission's Microwave Imager (TRMM-TMI), the Advanced Microwave Scanning Radiometer-Earth Observing System (AMSR-E) and WindSat (Owe et al., 2008; Parinussa, Holmes, & De Jeu, 2011a), and has been demonstrated to generate good quality θ estimates (Gruhier et al., 2010; Rossato, De Jeu, Alvala, & Souza, 2011; Rudiger et al., 2009; Su, Ryu, Young, Western, & Wagner, 2013; Wagner, Naemi, Scipal, De Jeu, & Martinez-Fernandez, 2007). Unlike other θ retrieval methods, the LPRM simultaneously retrieves both θ and vegetation optical depth (τ_v , dimensionless) from microwave brightness temperatures (T_b in K) via inversion of the radiative transfer model. It therefore does not require prior external information on vegetation (Huulin, Wood, Drusch, Crow, & Jackson, 2004; Kerr et al., 2012; Meesters, De Jeu, & Owe, 2005).

In November 2009, ESA launched the Soil Moisture and Oceans Salinity (SMOS) satellite (Kerr et al., 2010); the first mission dedicated to soil moisture. It observes at the 1.4 GHz (L-band) frequency which is considered to be optimal for θ retrievals because of the low sensitivity to cloud and vegetation contamination, a thermal sampling depth of several centimeters, and a high sensitivity to soil moisture fluctuations (Njoku & Entekhabi, 1996). SMOS is the first of several satellite missions measuring at L-band; in 2011 Aquarius (Le Vine, Lagerloef, Colomb, Yueh, & Pellerano, 2007b) was launched, and the Soil Moisture Active Passive (SMAP) mission (Entekhabi et al., 2010) is launched in 2015. The spatial resolution of the current SMOS Level 3 soil moisture product (SMOS L3) is 43 km. The unique capabilities of SMOS make it desirable to include retrievals from the sensor in ESAs long-term soil moisture climate record. To maintain consistency in the CCI data record, arguably application of the LPRM algorithm to derive θ from SMOS may be more preferable than to use the SMOS L3 product produced by alternative algorithms. In particular, (a) the other passive microwave θ retrievals in the long-term record are derived by the LPRM, (b) the SMOS L3 produces soil moisture for the dominant land type rather than an area-averaged soil moisture estimate for the entire footprint, which introduces conceptual differences and (c) LPRM uses as little as possible ancillary data, which is highly desired for the CCI θ dataset (De Jeu et al., 2014).

LPRM has not yet been thoroughly tested in combination with L-band measurements. De Jeu, Holmes, Panciera, and Walker (2009) showed promising results applying LPRM to L-band observations and ground data from the National Airborne Field Experiment 2005 (NAFE05) over southeast Australia, but stressed that verification with satellite observations was needed, especially because of the lesser incidence angles (up to 40°) and the higher radiometric accuracy (<0.7 K) of the airborne data, when compared to SMOS observations (up to 65° and 2.5–3 K, respectively). LPRM has typically been applied to incidence angles between 50–55° and the applicability of LPRM for a wider range of incidence angles, such as those available from SMOS, has not yet been tested. Like most θ retrieval methods, LPRM requires an estimate of the effective soil temperature (T_{eff} in K) as input to the retrieval scheme. For multi-channel observations, T_{eff} may be inferred from higher frequency channels (e.g. AMSR-E 37 GHz vertical polarized brightness temperature; Holmes, De Jeu, Owe, & Dolman, 2009). However the SMOS (and SMAP) sensors only have a single frequency radiometer at 1.4 GHz, and therefore ancillary temperature data are

needed for θ estimation. To address this, two methods to estimate T_{eff} from model simulated land surface temperature have been proposed: (1) by applying a phase-shift and amplitude reduction to a temperature dataset (Holmes, Jackson, Reichle, & Basara, 2012; Parinussa, Holmes, Yilmaz, & Crow, 2011b) and (2) as a function of the surface skin temperature (T_{surf}), deep soil temperature (T_{deep}) and θ (De Rosnay, Wigneron, Holmes, & Calvet, 2006; De Rosnay et al., 2006; Wigneron, Laguerre, & Kerr, 2001), which is in line with the SMOS L3 product. In this study, two objectives are addressed:

1. Establish the quality of LPRM θ retrievals from SMOS L-band observations over the Murrumbidgee catchment and compare this with SMOS L3 θ retrievals;
2. Understand the dependence of retrieval quality on incidence angles of 45° to 60° and on the time of overpass.

To test the parameterization of the LPRM and to evaluate its retrieval outputs ground-based data of the Murrumbidgee Soil Moisture Monitoring Network (OzNet) in southeast Australia was used, because of its dense ground observation network, the variety in land cover types and its applicability to remote sensing studies (Smith et al., 2012).

2. Data and preprocessing

2.1. SMOS

The SMOS satellite carries the Microwave Imaging Radiometer with Aperture Synthesis (MIRAS); a two-dimensional interferometric radiometer that measures the passive radiation emitted by the Earth's surface at the L-band frequency (1.4 GHz). The satellite is in a polar sun-synchronous orbit with a distance of around 758 km from the Earth. The measurements are made for incidence angles between 0° and 65° (Kerr et al., 2010), have an average ground resolution of 43 km and a swath width of 1000 km in the alias-free field of view (Camps, Vall-llossera, Corbella, Duffo, & Torres, 2008). One full measurement is made every 1.2 s, in X, Y or XY polarization in the instrument's reference frame, which differs from horizontal (H) and vertical (V) polarization at surface level. The satellite has a maximum revisit time of 3 days for a fixed point at the ground in case radiometric error is not considered for filtering, with a 6:00 a.m. (local time) ascending and 18:00 p.m. descending overpass (Kerr et al., 2012).

In this study brightness temperatures from the SMOS Level 1C Full-polarization (SCLF1C) data product version 505 for January 2010 until December 2011 were used. The level 1C land product contains multi-angular brightness temperatures at the top of the atmosphere, is georeferenced and provided in the ISEA-4H9 grid format, with an average ground sampling interval of 15 km. The data is organized in files that contain half an orbit and are still in X/Y/XY polarization.

The measurements with incidence angles within $\pm 0.4^\circ$ of 45°, 52.5° and 60° were extracted from the data. These were selected to test the performance of LPRM for different incidence angles, with 52.5° being a value extensively tested for LPRM (Owe et al., 2008). The incidence angles are kept above 40° due to the higher sensitivity of H-polarized measurements to soil moisture while V-polarized measurements are strongly affected by T_{eff} at high incidence angles. The data were transformed from X/Y/XY to H/V/HV measurements by correcting for Faraday and geometric rotations following Le Vine, Jacob, Dinnat, de Matthaeis, and Abraham (2007a). This method theoretically needs measurements that are made at the same time and incidence angle, which is practically impossible since each SMOS observations cover a unique area only in one polarization. To solve this and minimize the introduced error, only a full set of measurements (X, Y and XY polarized) made within 3 s for the same grid point were selected, ensuring that the measurements were near coincident in time with a maximum difference in incidence angle of 0.7° for the transformations (Le Vine et al., 2007a).

The data in ISEA-4H9 grid format were resampled to a regular 0.25° grid using area-weighted averaging to allow comparison to field data

following Su et al. (2013), the input and regridded data are assumed to be of identical quality (Dumedah, Walker, & Rüdiger, 2014). Measurements with reported radiometric T_b error exceeding 3 K or located outside the alias-free field of view (Camps et al., 2008) were excluded. This threshold was used because the retrievals, particularly those at 45°, proved to be very sensitive to larger errors. The exclusion of measurements with high radiometric errors caused a considerable increase in the quality of the resulting 45° retrievals, with an increase in Pearson's coefficient of correlation (r) of 0.08 on average, and a decrease of the root mean square error (RMSE) of $0.02 \text{ m}^3 \text{ m}^{-3}$. Due to the different swath width for each incidence angle, removal of observations with high errors and availability of temperature datasets, the amount of SMOS observations (N) used in the analyses varies.

The results of the SMOS LPRM retrievals were also directly compared to SMOS L3 θ , which was resampled to a 0.25° grid using area-overlap weighted averaging. The re-processed (version RE02) data were obtained from the Centre Aval de Traitement des Données SMOS (CATDS), operated for the "Centre National d'Etudes Spatiales" (CNES) by IFREMER (Brest, France).

2.2. MERRA land surface temperature

Holmes et al. (2012) assessed the ability of three numerical weather prediction models to provide T_{eff} estimates that meet the requirements for L-band θ retrieval models and found that T_{surf} from the Modern-Era Retrospective analysis for Research and Applications (MERRA) atmospheric reanalysis system was most suitable as input for their method. This was induced by the high temporal resolution of this reanalysis product resulting in a relatively low RMSE (1.8 K) for morning overpasses compared to in situ soil temperature measurements. Parinussa et al. (2011b) further demonstrated that applying this method with MERRA T_{surf} on LPRM retrievals from WindSat and AMSR-E produced good results, with a slightly lower performance in resulting θ retrievals for sparsely vegetated areas and better performance for moderately to heavily vegetated areas compared to a radiometric based T_{eff} product. Their comparison was done at the quasi-global scale using the R_{value} approach (Crow & Van den Berg, 2010) as well as the Triple Collocation technique (Dorigo et al., 2010).

MERRA is developed by the National Aeronautics and Space Administration (NASA) and produces global estimates of geophysical variables such as θ , latent heat flux, snow and runoff. The data are generated by a recent version of the Goddard Earth Observing System, version 5 (GEOS-5) and are covering a period of 1979 to present (Rienecker et al., 2011). T_{surf} data from MERRA-Land reanalysis was used, which is a land only, revised and off-line run of the standard MERRA. It contains several additional variables including T_{surf} and has shown improved performance over land compared to the standard MERRA model, because it was revised and rerun using a more realistic precipitation forcing and parameterization (Reichle, 2012; Reichle et al., 2011). MERRA-Land data are available on a $0.5 \times 0.67^\circ$ grid with hourly resolution, representing average hourly temperature for the soil surface of negligible depth except for tropical forests (Reichle, 2012). Data for the period July 2009–June 2012 were downloaded from <http://gmao.gsfc.nasa.gov/merra/>.

2.3. ECMWF temperature

The second method for deriving T_{eff} (De Rosnay & Wigneron, 2005; Wigneron et al., 2001) uses temperature forecasts from the European Centre for Medium-Range Weather Forecasts (ECMWF) and is the method used for the SMOS L3 product. The ECMWF forecasting system consists of several parts, including The Hydrology-Tiled ECMWF Scheme for Surface Exchange over Land (H-TESSEL) (Balsamo et al., 2009). H-TESSEL is a land surface model that calculates the heat, water and momentum exchanges between the atmosphere and the different components of the land surface. These components include

the soil skin, a four-layer soil profile, the land cover and, if present, the snowpack. In this study, the AUX_ECMWF product generated specifically as auxiliary input for the SMOS L3 product was used from July 2010 to December 2011. This product is spatially and temporally interpolated to match with the SMOS time of overpass and grid. For the T_{eff} estimation, T_{surf} and T_{deep} from the soil layer of 0.21–0.72 m depth are used. The data was regridded from the ISEA grid to a 0.25° grid using area-overlap weighted averaging.

2.4. Field observations

Field θ observations from the OzNet network (Smith et al., 2012) in the Murrumbidgee catchment in southeast Australia were also used. The Murrumbidgee River drains a catchment of approximately 82,000 km² and is the third largest river in the Murray–Darling basin. The catchment has varying topography (low-lying plains to the west, alpine mountains in the east), climate (annual rainfall from 400 mm in the west to 1400 mm in the east) and land use (cropping and grazing, to forestry and national parks).

OzNet is a network of in situ moisture probes at 62 sites across the Murrumbidgee catchment, (<http://www.oznet.org.au/>; Smith et al., 2012). Moisture measurements are acquired every 30 min at various depths down to ca. 0.9 m. Here θ measurements closest to the time of satellite overpass were used. The θ observations that correspond to the top 0.08 m were measured with a CS615 probe (older sites) and 0.05 m were measured with a Stevens Hydra probe (newer sites).

In this study the same OzNet dataset is used as in Su et al. (2013), in which they identified 49 good quality sites and grouped them into 17 cells on a 0.25° regular grid for comparison against the AMSR-E, ASCAT (Advanced Scatterometer of MetOp-A satellite) and SMOS soil moisture products (Table 1). This was done by Su et al. (2013) by removing single sites that provide anomalous evaluation results compared to the average results of all the sites within that grid cell. Data for the period of January 2010 to December 2011 was used here, the Adelong Creek site was excluded because of data availability issues from early 2010 onwards leaving too few observations for analysis. For a comprehensive description of preprocessing of the ground data and the data set used in this study see Su et al. (2013).

3. Methods

3.1. The land parameter retrieval model

The LPRM (De Jeu et al., 2014; Owe et al., 2001; Owe et al., 2008) is developed to retrieve land surface parameters from passive microwave observations. It is based on a forward model that uses horizontally and

Table 1

Summary of the grid cells used for the ground observations, from Su et al. (2013).

Site	Latitude (°E)	Longitude (°S)	Measurements sites in the grid cell	Land use
M-1	148.875	−36.375	1	Forest
M-2	149.125	−35.375	1	Urban (city of Canberra)
M-3	148.125	−34.625	1	Agriculture
M-4	147.125	−33.875	1	Agriculture/Forest
M-5	143.625	−34.625	1	Forest
M-6	144.875	−34.625	1	Agriculture/Grass
M-7	146.125	−34.125	1	Agriculture/Forest
Y-1	145.875	−34.625	1	Agriculture/Forest
Y-2	146.125	−34.625	12	Agriculture/Forest
Y-3	146.375	−34.625	2	Agriculture/Forest/Urban
Y-6	145.875	−34.875	1	Agriculture
Y-9	146.125	−34.875	3	Agriculture
Y-B	146.375	−34.875	7	Agriculture
Y-10	146.375	−35.125	4	Agriculture
K-1	147.625	−35.375	6	Agriculture/Forest
K-14	147.375	−35.125	1	Agriculture/Urban
A	148.125	−35.375	5	Forest

vertically polarized microwave brightness temperature ($T_{b(P)}$ in K, where P is H for horizontal or V for vertical polarization) and T_{eff} to simultaneously solve for θ and τ_v . The basis of the model is the radiative transfer theory of Mo, Clough, Schmugge, Wang, and Jackson (1982), which describes the $T_{b(P)}$ emission of an area measured above canopy level as

$$T_{b(P)} = e_{r(P)} T_{eff} \Gamma_v + (1-\omega) T_C (1-\Gamma_v) + (1-e_{r(P)}) (1-\omega) T_C (1-\Gamma_v) \Gamma_v \quad (1)$$

where ω is the single scattering albedo, Γ_v the vegetation transmissivity, $e_{r(P)}$ the rough surface emissivity for H- or V-polarized radiation (all dimensionless) and T_C (in K) the canopy temperature, which is assumed equal to the effective soil temperature (T_{eff}). Because at L-band wavelengths the atmospheric contribution to the signal is very small (Kerr et al., 2012), atmospheric opacity is assumed to be 0.

The value of $e_{r(P)}$ is determined in three steps. First, the dielectric constant of the soil is calculated through the dielectric mixing model of Wang and Schmugge (1980), which requires soil porosity, wilting point, T_{eff} and θ as input. Values of soil porosity and wilting point are derived from the FAO soil texture map (Reynold, Jackson, & Rawls, 1999). Second, the absolute value of the dielectric constant (k) and incidence angle (u in radians) are combined with the Fresnel equations to calculate the smooth surface reflectivity for both polarizations ($R_{(P)}$). Third, the model of Wang and Choudhury (1981) is used to calculate $e_{r(P)}$

$$e_{r(P1)} = 1 - \left((1-Q) R_{(P1)} + Q R_{(P2)} \right) e^{-h \cos u} \quad (2)$$

where Q is the polarization mixing factor, $P1$ and $P2$ the two polarizations, and h a dimensionless roughness. Finally, the value of Γ_v in the radiative transfer model (Eq. 1) is defined as

$$\Gamma_v = \exp\left(\frac{-\tau_v}{\cos u}\right). \quad (3)$$

LPRM uses the analytical formula by Meesters et al. (2005) and the Microwave Polarization Difference Index (MPDI) to calculate τ_v at nadir as

$$\tau_v = \cos u \ln \left(ad + \sqrt{(ad)^2 + a + 1} \right) \quad (4)$$

where

$$a = 0.5 \left(\frac{e_{r(V)} - e_{r(H)}}{\text{MPDI}} - e_{r(V)} - e_{r(H)} \right) \quad (5)$$

$$d = 0.5 \left(\frac{\omega}{1-\omega} \right) \quad (6)$$

$$\text{MPDI} = \frac{T_{b(V)} - T_{b(H)}}{T_{b(V)} + T_{b(H)}} \quad (7)$$

The analytical solution for τ_v is based on the assumption that τ_v is independent of polarization, which is generally considered a reasonable assumption for microwave observations from satellite platforms (De Lannoy, Reichle, & Pauwels, 2013; Owe et al., 2001). Soil moisture is retrieved by applying the LPRM model in forward mode for a range of θ conditions. The resulting $T_{b(H)}$ simulations are compared to the satellite observed value and the θ resulting in the smallest residual is selected as the best estimate.

3.2. Parameterization for the L-band frequency

Three parameters have to be determined in order to make the LPRM applicable to L-band microwave observations: Q , h and ω . The

polarization mixing factor, Q , has been assumed very small for L-band (Wigneron et al., 2001), with commonly suggested values below 0.1 and often zero; hence Q values of 0 to 0.1 were tested.

At higher frequencies the roughness factor (h) describes the geometric roughness of the land surface. At L-band, h depends more on the distribution of water in the soil than at higher frequencies and can be described as an apparent soil roughness (Schneeberger et al., 2004). This makes h a dynamic variable that varies in time and space. Several dynamic parameterizations of h have been proposed by Escorihuela et al. (2007), Kerr et al. (2012), Panciera et al. (2009) and De Jeu et al. (2009). In this study h is expressed as a function of θ and two scaling parameters h_1 and h_2 as

$$h = h_1 - h_2 * \theta. \quad (8)$$

Several studies showed that h can assume high values when used to interpret SMOS observations, with reported values of nearly 2 (De Lannoy, Reichle, & Vrugt, 2014; De Lannoy et al., 2013 and Sabater, Rosnay, & Balsamo, 2011). Therefore h_1 values of 0 to 2, and h_2 values of up to 4 times the used h_1 value were tested.

The literature appears divided on appropriate assumptions about the single scattering albedo, ω . Some studies suggest that the value is typically low enough to be ignored to allow simplification of the radiative transfer equation (Eq. 1), while others find values typically between 0.05 and 0.15, but varying in time and space (Van de Griend & Wigneron, 2004; Wigneron et al., 2004). Furthermore, it is plausible that ω depends on the incidence angle. Values of 0 to 0.2 were tested here to cover the existing range presented in literature.

The model parameters Q , h and ω were adapted in order to optimize the remotely sensed soil moisture product with ground observations through maximizing the correlation and minimizing the RMSE between the estimated and observed θ . Sensitivity tests were carried out and visualized in Taylor diagrams (Taylor, 2001) to test the influence of parameter uncertainty on retrieved θ and to identify the more critical model parameters.

3.3. Effective soil temperature processing

3.3.1. MERRA-land

Another source of information required in the radiative transfer Eq. (1) is the T_{eff} . MERRA T_{surf} represents the temperature at, or very close to, the soil surface, while the observed L-band radiation is emitted from a thicker layer; theoretically ranging between 0.015 m and 0.15 m depending on θ content at 50° incidence angle (Ulaby, Moore, & Fung, 1986). To account for this difference, the method of Holmes et al. (2012) is applied to estimate soil temperature at 0.05 m depth and assuming that to be the T_{eff} .

In this method the amplitude reduction and phase-shift are linked to the downward propagation of periodic temperature variations. The theory for this, assuming a stable temperature at depth and conductive heat transfer, was described by Van Wijk and De Vries (1963). Holmes et al. (2012) found that using a phase-shift of 169 min, and its associated amplitude reduction, produced the best agreement with the soil temperature at 0.05 m depth in a dense ground measurements network in Oklahoma, USA. For this study the same phase-shift of 169 min was applied on the MERRA T_{surf} data. It should be noted that at very low soil moisture levels the diffusivity is so low that the heat only dissipates slowly in the soil, which theoretically leads to a much larger phase-shift (Holmes et al., 2012) that is not corrected for in this method. A detailed description on the used method can be found in Holmes et al. (2012).

Splines were used to interpolate and estimate T_{eff} at the time of the satellite overpass over the OzNet area. The estimates were subsequently resampled to a regular 0.25° grid using area-weighted averaging for grid cells covered by two grid cells in the original MERRA-Land 0.5 × 0.67°

Table 2
Optimized LPRM parameters per incidence angle.

Incidence angle	ω	h	Q
45°	0.18	1.0–3.5 * θ	0
52.5°	0.165	1.4–4.9 * θ	0
60°	0.15	1.8–6.3 * θ	0

grid. Measurements with $T_{eff} < 273.15$ K ($N = 7$) were removed, since the retrieval model is not valid for these conditions.

3.3.2. ECMWF

The second method uses a different approach to estimate the T_{eff} and was developed by Wigneron et al. (2001), and validated and revised by De Rosnay and Wigneron (2005). It is based on a simple parameterization to estimate T_{eff} for passive microwave radiometry formulated by Choudhury, Schmugge, and Mo (1982). The T_{eff} here is calculated using T_{surf} and T_{deep} (at a depth where it is mainly stable) using a fitting parameter C that depends on θ and two constants w_0 and b :

$$T_{eff} = T_{surf} + C * (T_{surf} - T_{deep}) \quad (9)$$

where

$$C = \left(\frac{\theta}{w_0} \right)^b. \quad (10)$$

The values for w_0 and b used in this study are identical to those used in the SMOS L3 algorithm, $0.3 \text{ m}^3 \text{ m}^{-3}$ and 0.3 respectively. Since LPRM is applied in forward mode for a range of θ conditions, a corresponding T_{eff} is calculated for all the individual θ scenarios.

3.4. Evaluation techniques

Three bivariate statistical measures were used to evaluate the retrieved θ estimates against the ground measurements: Pearson's coefficient of correlation (r), mean bias and root mean square error (RMSE). A caveat is that there can be important conceptual differences between satellite derived and ground observed soil moisture: they have different spatial support (point vs. footprint), vertical support (in situ sensor vs.

microwave emitting layer) and differences in the time of acquisition (Owe et al., 2001).

The confidence interval (CI) for the r , as used in Tables 3, 4 and 5, was calculated using Fisher's transform with a 95% confidence level. The CI for the bias was calculated as

$$CI_{bias} = \sqrt{\left(\frac{z^2}{N} \right) (\sigma_r^2 \sigma_R^2)} \quad (11)$$

with critical value $z = 1.96$, while N is the length of the time series, and σ_r and σ_R the standard deviations of the in situ and remote sensed time series, respectively. In order to propagate the confidence interval from the single sites to the total result, the sum of all the CI values per site was divided by the square root of the number of sites (i.e., 16).

4. Results and discussion

4.1. Adjusting LPRM for L-band, parameterization

The optimized parameters of h , Q and ω are listed in Table 2. Optimal values of ω ranged between 0.15 and 0.18, decreasing with incidence angle. The optimal Q was 0 in all cases, which is in line with findings of Wigneron et al. (2001). Given the h parameterization in Eq. (8), h_1 values were optimal from 1.0 to 1.8, with increasing incidence angle, and similarly for h_2 that valued from 3.5 to 6.3 (3.5 times h_1). All three parameters were independent of acquisition time and apply to both the MERRA and ECMWF using their respective temperature conversion methods (Sections 3.3.1 and 3.3.2). It is reiterated that these values were optimized for the OzNet pixels, and are not necessarily optimal elsewhere as systematic error in T_{eff} may vary spatially (Parinussa et al., 2011b).

To analyze the sensitivity of the LPRM parameterization on θ retrievals, the values of r , RMSE, standard deviation and bias of the θ retrievals are shown in Fig. 1, representing scenarios in which one parameter is changed while all others are kept constant at their optimized value (Table 2). Fig. 1 shows the optimization effect for the cell of Y-B, which was chosen as an example representative for all evaluated sites. The h is shown in the form of h_1 used in Eq. (8) with $h_2 = 3.5 h_1$.

Variation in ω showed to have the most significant impact on LPRM θ retrievals, with r values changing from <0.5 to 0.8 for 45° and 52.5°

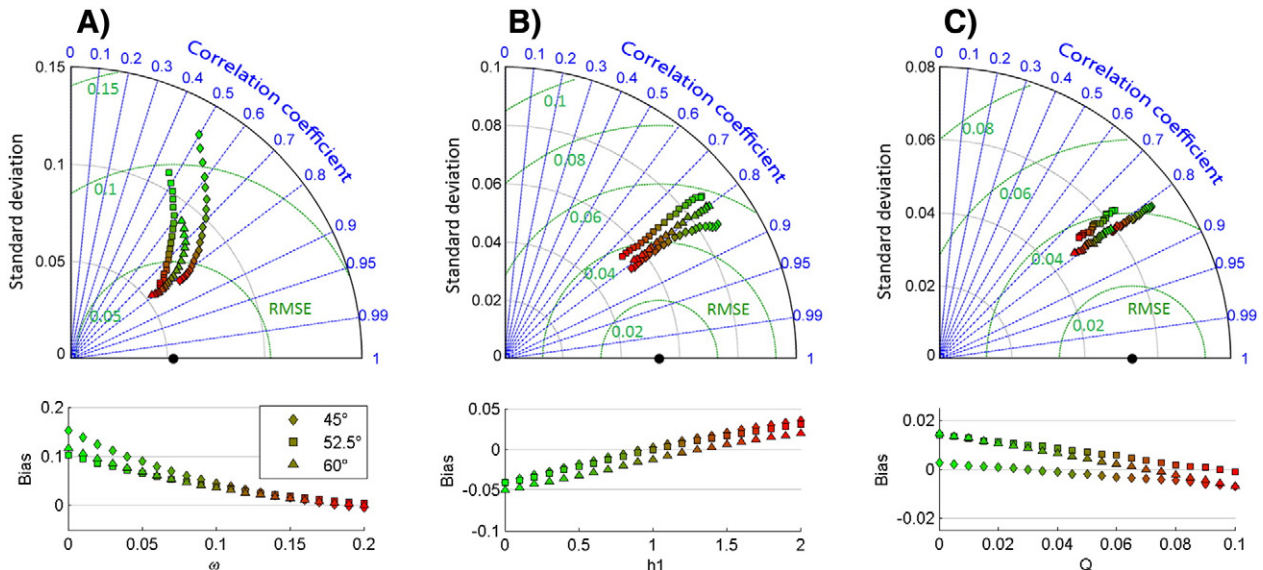


Fig. 1. Taylor diagrams and bias over site Y-B when optimizing for single scattering albedo (A), roughness (B) and polarization mixing (C), using both ascending and descending data with MERRA T_{eff} and where the green to red coloring of the markers corresponds to an increasing parameter value.

Table 3
Results of the optimized LPRM θ retrievals compared to the 16 OzNet grid cells (Table 1).

	Incidence angle	Swaths	$r \pm CI$	RMSE [$m^3 m^{-3}$]	Bias $\pm CI$ [$m^3 m^{-3}$]	N
MERRA	45°	Ascending	0.70 \pm 0.47	0.085	-0.01 \pm 0.09	1415
		Descending	0.71 \pm 0.49	0.078	0 \pm 0.10	1189
	52.5°	Ascending	0.71 \pm 0.44	0.074	-0.01 \pm 0.08	1507
		Descending	0.74 \pm 0.46	0.071	0.01 \pm 0.09	1152
	60°	Ascending	0.72 \pm 0.43	0.075	0 \pm 0.08	1424
		Descending	0.71 \pm 0.58	0.073	0.01 \pm 0.10	921
Mean	Ascending	0.74 \pm 0.45	0.074	-0.01 \pm 0.09	1288	
	Descending	0.75 \pm 0.52	0.070	0.01 \pm 0.10	864	
ECMWF	45°	Ascending	0.72 \pm 0.51	0.081	-0.02 \pm 0.10	1133
		Descending	0.74 \pm 0.52	0.076	-0.01 \pm 0.10	953
	52.5°	Ascending	0.73 \pm 0.47	0.073	-0.02 \pm 0.08	1215
		Descending	0.74 \pm 0.53	0.070	0 \pm 0.10	906
	60°	Ascending	0.75 \pm 0.45	0.074	-0.01 \pm 0.09	1146
		Descending	0.70 \pm 0.67	0.073	0 \pm 0.11	720
Mean	Ascending	0.77 \pm 0.46	0.072	-0.01 \pm 0.09	1035	
	Descending	0.76 \pm 0.58	0.069	0 \pm 0.11	679	

incidence angle and from 0.6 to 0.8 for 60° after increasing ω from 0 to 0.2. The ω variation also resulted in a significant decrease of RMSE (>0.1 to $0.04 m^3 m^{-3}$ for 45° and 52.5° incidence angle and 0.08 to $0.04 m^3 m^{-3}$ for 60°) and standard deviation (from 0.13, 0.11 and 0.09 to 0.07, 0.06 and $0.05 m^3 m^{-3}$ for 45°, 52.5° and 60°) and a drop in bias of more than $0.10 m^3 m^{-3}$. Optimization of Q had no influence on r , hardly impacted the RMSE and resulted in a slight decrease of the standard deviation. An increase in h also resulted in a decrease in standard deviation, improved the RMSE and produced a wetter bias. These results suggest that the skill of LPRM θ retrievals is mostly impacted by the ω parameter. The obtained sensitivity results may not necessarily be transferable to other retrieval algorithms as the LPRM is more

heavily influenced by the ω compared to other retrieval algorithms, this is likely due to the influence of ω on the vegetation effects in both Eqs. (1) and (4) to (7) when τ_v is calculated following Meesters et al. (2005).

4.2. LPRM soil moisture retrievals compared to OzNet

Comparison of the LPRM retrievals against ground measurements revealed comparable results (Table 3 and Fig. 2) for the three different incidence angles, the descending and ascending data and both T_{eff} approaches (using MERRA and ECMWF). Mean r values were between 0.70 and 0.75, mean bias -0.02 to $0.01 m^3 m^{-3}$ and mean RMSE 0.070 to $0.085 m^3 m^{-3}$ for optimal parameters. Agreement for the simple average of the retrievals from the three incidence angles (when all are available) shows slightly improved results for r up to 0.77 (Table 3), these combined estimates are shown in Fig. 2.

Although the results are comparable, small differences for the three incidence angles are present. The retrievals for 52.5° and 60° are generally similar, with those at 52.5° showing the best performance in terms of RMSE. The RMSE values of the retrievals for the 45° incidence angle are consistently higher compared to the other incidence angles, however it's just a small difference (on average $0.007 m^3 m^{-3}$). It is suggested that LPRM loses sensitivity to soil moisture at lower incidence angles, caused by the smaller contrast between $T_{b(H)}$ and $T_{b(V)}$, used in the MPDI (Eq. 7), therefore it is likely that the model becomes more sensitive to errors in the input values. This was also the reason to remove SMOS observations with uncertainties exceeding 3 K from the analysis (Section 2.1). This decrease in stability can also be seen in the LPRM τ_v retrievals at 45°, showing more outliers (Fig. 3F for cell Y-B, but applies to all cells). These effects of input errors on τ_v retrievals are known for LPRM and for example described by Liu, De Jeu, McCabe, Evans, and

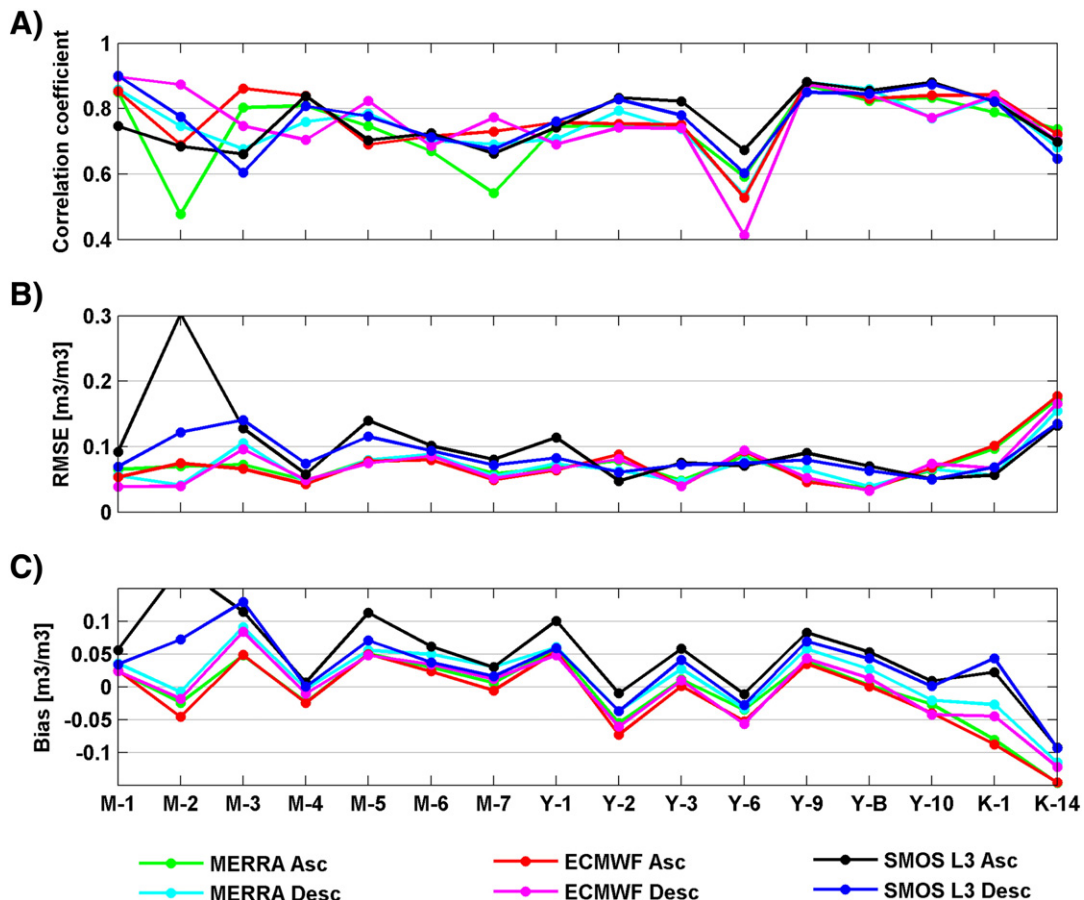


Fig. 2. Evaluation statistics per grid cell, the MERRA and ECMWF datasets are the average of the three different incidence angles, showing the r (A), RMSE (B) and bias (C).

Van Dijk (2011), Liu, Van Dijk, McCabe, Evans, and De Jeu (2012b) and De Jeu (2003).

Only minor differences between the ascending and descending overpasses were presented in the averaged results. The RMSE for the ascending overpass is consistently higher than for the descending overpass for the same incidence angles, and the descending estimates had a slight wet bias against the ascending estimates ($0.01\text{--}0.02\text{ m}^3\text{ m}^{-3}$). Some individual sites revealed better results for the ascending than for the descending data (e.g., M-3; see Fig. 3) but the opposite also occurred

(e.g., M-2). It is noted, however, that site M-2 contains the city of Canberra, which could lead to increased T_b uncertainties due to the high fraction of urban land cover (Ye, Walker, Rudiger, Ryu, & Gurney, 2011) and possible radio frequency interference (RFI) from major military and space communication installations, while it is also surrounded by mountains.

Despite using a very different approach to estimate T_{eff} , the two different temperature methods also produced similar results. The ECMWF method produced on average slightly higher r ($+0.01\text{ m}^3\text{ m}^{-3}$) and

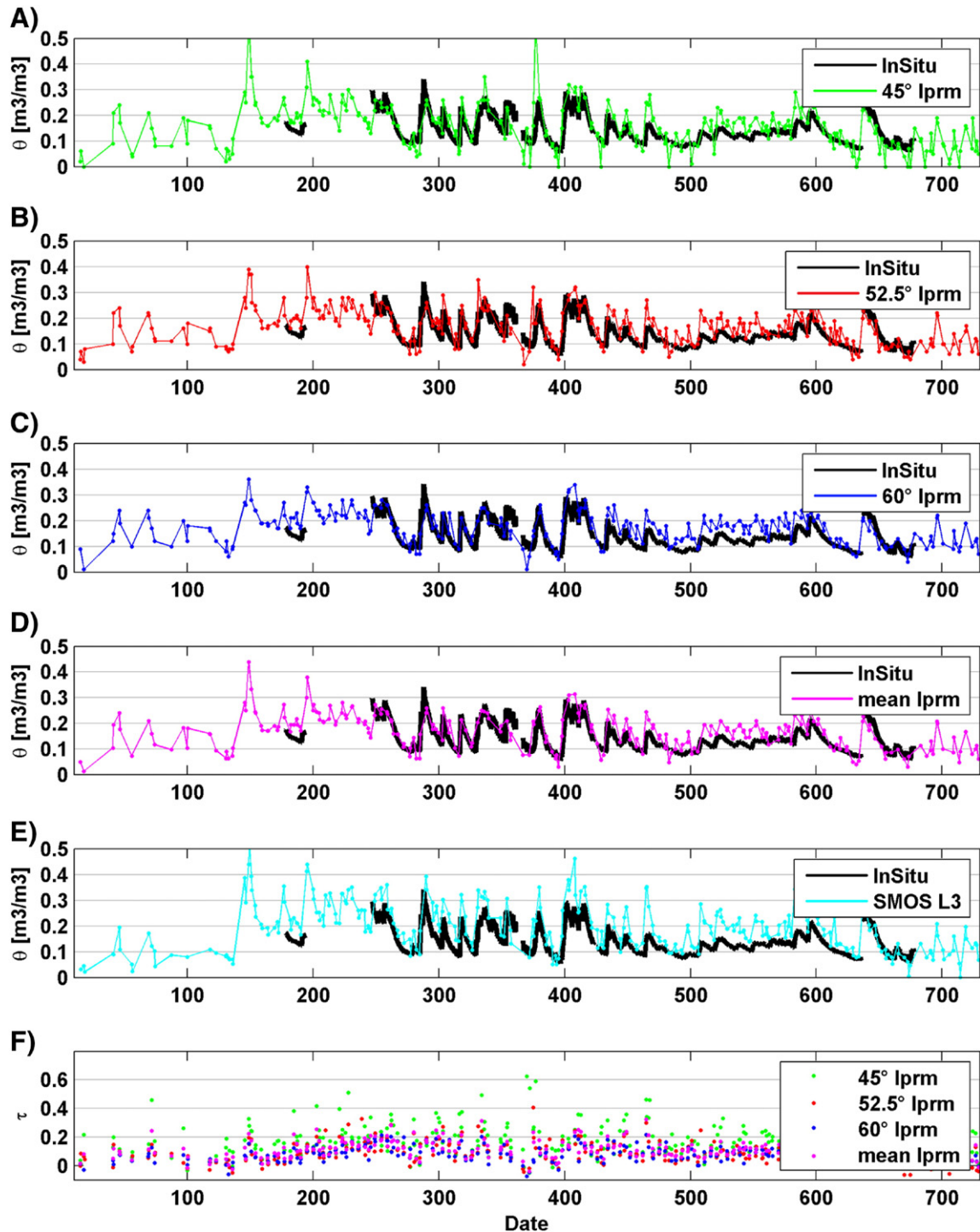


Fig. 3. Time series of ascending and descending soil moisture retrievals against the ground measurements and vegetation optical depth for cell Y-B, with LPRM θ retrievals for the different incidence angles and mean LPRM (A to D), SMOS L3 θ retrievals (E) and the LPRM τ_v (F). Date in days from 1/1/2010 onwards.

lower RMSE ($-0.02 \text{ m}^3 \text{ m}^{-3}$), but the differences are not significant. For single cells, the results were inconsistent. For example, at M-7 ECMWF produced higher r values, whereas at Y-6 MERRA performed better. A more comprehensive comparison for individual sites is provided in the [Supplementary material](#).

In summary, with optimized parameters LPRM is able to retrieve good quality ($r \geq 0.7$) soil moisture estimates over OzNet using single-angle L-band observations of SMOS. The influence of the time of overpass, incidence angle, and temperature estimation method appears to be small, and therefore all options appear to be feasible in further studies on applying LPRM to SMOS observations. The ability to optimize SMOS LPRM to good correlations ($r \geq 0.7$) also suggests once again that the OzNet network is a good representation of the regional soil moisture dynamics in the Murrumbidgee Catchment (Smith et al., 2012).

4.3. LPRM soil moisture retrievals compared to SMOS L3

Comparing the optimized SMOS LPRM retrievals to the SMOS L3 retrievals suggests that their average quality is similar (Table 4). In terms of correlation, SMOS L3 always performed slightly better (0.01–0.06) but the RMSE was higher (0.011–0.030 $\text{m}^3 \text{ m}^{-3}$). When looking at the simple average of the LPRM retrievals from the three incidence angles the difference in r becomes smaller (0–0.03). The main reason for the higher RMSE in SMOS L3 ascending data is due to the fact that SMOS L3 is not calibrated for OzNet and the Canberra site (M-2, Table 4), where SMOS L3 soil moisture retrievals are overestimated. The overall higher RMSE in the SMOS L3 retrievals is mainly the result of a wet bias, $0.05 \text{ m}^3 \text{ m}^{-3}$ for the ascending and $0.03 \text{ m}^3 \text{ m}^{-3}$ for the descending dataset, over study area. The LPRM algorithm seems to compensate the potential error sources (urban cover, RFI, mountains) in M-2 by calculating unrealistically high τ_v with much variation, for the rest of the study area obtained results are very similar.

When comparing the SMOS L3 directly to the LPRM retrievals, correlations are high for both with r values between 0.82 and 0.88, increasing to up to 0.92 when comparing the average LPRM retrievals to SMOS L3 (Table 5). The RMSE is still quite large, between 0.051–0.092 $\text{m}^3 \text{ m}^{-3}$. The bias shows clear differences for the time of overpass: the LPRM soil moisture retrievals show dry biases compared to the SMOS L3 product for both overpasses, the ascending overpass show somewhat larger bias values (between 0.05 and $0.07 \text{ m}^3 \text{ m}^{-3}$) than the descending overpass ($<0.05 \text{ m}^3 \text{ m}^{-3}$). The similar performance of SMOS LPRM compared to the SMOS L3 soil moisture product, for both the comparison to the OzNet site as directly compared to each other, shows that SMOS LPRM is able to retrieve soil moisture estimates from single angle L-band observations of the SMOS satellite.

5. Conclusion and outlook

This work demonstrated that the LPRM is capable of retrieving soil moisture estimates over OzNet using single-angle L-band observations by the SMOS satellite of equivalent quality when compared to alternative methods and products. We focused our comparison on the official SMOS L3, but existing literature (Su et al., 2013) also suggests a comparable performance against other remotely sensed soil moisture products (ASCAT and AMSR-E LPRM). Optimization and evaluation against OzNet in situ observations produced mean r values of 0.70–0.75 (0.75–0.77 for SMOS L3), mean bias of -0.02 to $0.01 \text{ m}^3 \text{ m}^{-3}$ (0.03 – $0.06 \text{ m}^3 \text{ m}^{-3}$ for SMOS L3) and mean RMSE of 0.070 to $0.085 \text{ m}^3 \text{ m}^{-3}$ (0.084 – $0.106 \text{ m}^3 \text{ m}^{-3}$ for SMOS L3). Incidence angle, time of overpass and the use of the MERRA or ECMWF temperature method did not exert a large influence on retrieval quality. A major advantage of the SMOS LPRM approach is that it minimizes the use of ancillary data (i.e. only the FAO soil map and T_{eff} are used to convert the dielectric constant into soil moisture values) which is an important requirement for climate studies (De Jeu et al., 2014).

Table 4

Direct comparison between SMOS LPRM θ and the regridded SMOS L3 θ product over the same SMOS observations using OzNet θ measurements as a reference.

Angle	Temperature	Swath	L3/LPRM	$r \pm \text{CI}$	RMSE [$\text{m}^3 \text{ m}^{-3}$]	Bias $\pm \text{CI}$ [$\text{m}^3 \text{ m}^{-3}$]	N
45°	MERRA	Ascending	L3	0.77 ± 0.38	0.102	0.05 ± 0.11	1330
			LPRM	0.70 ± 0.47	0.085	-0.01 ± 0.10	1330
	ECMWF	Descending	L3	0.75 ± 0.41	0.089	0.03 ± 0.11	1146
			LPRM	0.71 ± 0.49	0.078	0.00 ± 0.10	1146
		Ascending	L3	0.76 ± 0.44	0.106	0.06 ± 0.11	1082
			LPRM	0.72 ± 0.51	0.081	-0.02 ± 0.10	1082
52.5°	MERRA	Ascending	L3	0.76 ± 0.36	0.100	0.05 ± 0.10	1418
			LPRM	0.71 ± 0.44	0.074	-0.01 ± 0.08	1418
	ECMWF	Descending	L3	0.77 ± 0.40	0.086	0.03 ± 0.11	1110
			LPRM	0.75 ± 0.46	0.071	0.01 ± 0.09	1110
		Ascending	L3	0.76 ± 0.42	0.103	0.05 ± 0.11	1161
			LPRM	0.73 ± 0.47	0.073	-0.02 ± 0.08	1161
60°	MERRA	Descending	L3	0.76 ± 0.48	0.088	0.04 ± 0.11	883
			LPRM	0.74 ± 0.53	0.069	0.00 ± 0.09	883
	ECMWF	Ascending	L3	0.77 ± 0.37	0.101	0.05 ± 0.10	1337
			LPRM	0.72 ± 0.43	0.076	-0.01 ± 0.09	1337
		Descending	L3	0.77 ± 0.44	0.084	0.03 ± 0.12	896
			LPRM	0.71 ± 0.58	0.073	0.01 ± 0.10	896
Mean	MERRA	Ascending	L3	0.76 ± 0.42	0.105	0.06 ± 0.11	1095
			LPRM	0.75 ± 0.45	0.076	-0.01 ± 0.09	1095
	ECMWF	Descending	L3	0.77 ± 0.51	0.087	0.03 ± 0.13	712
			LPRM	0.70 ± 0.67	0.073	0.00 ± 0.11	712
		Ascending	L3	0.77 ± 0.40	0.102	0.05 ± 0.11	1212
			LPRM	0.74 ± 0.45	0.073	-0.01 ± 0.09	1212
Mean	MERRA	Descending	L3	0.77 ± 0.46	0.084	0.03 ± 0.12	840
			LPRM	0.75 ± 0.52	0.070	0.01 ± 0.10	840
	ECMWF	Ascending	L3	0.76 ± 0.46	0.105	0.06 ± 0.12	988
			LPRM	0.76 ± 0.46	0.073	-0.01 ± 0.09	988
		Descending	L3	0.77 ± 0.53	0.088	0.03 ± 0.13	671
			LPRM	0.76 ± 0.58	0.069	0.00 ± 0.11	671

Table 5
Direct comparison of SMOS L3 θ versus SMOS LPRM θ retrievals, using SMOS L3 as baseline.

	Incidence angle	Swaths	$r \pm CI$	RMSE [$m^3 m^{-3}$]	Bias $\pm CI$ [$m^3 m^{-3}$]	N
MERRA	45°	Ascending	0.83 \pm 0.20	0.086	-0.06 \pm 0.12	1330
		Descending	0.83 \pm 0.22	0.059	-0.03 \pm 0.11	1146
	52.5°	Ascending	0.84 \pm 0.16	0.080	-0.06 \pm 0.10	1418
		Descending	0.88 \pm 0.17	0.051	-0.02 \pm 0.10	1110
	60°	Ascending	0.83 \pm 0.18	0.082	-0.05 \pm 0.11	1337
		Descending	0.86 \pm 0.23	0.052	-0.01 \pm 0.12	896
Mean	Ascending	0.86 \pm 0.17	0.079	-0.06 \pm 0.12	1212	
	Descending	0.92 \pm 0.15	0.046	-0.02 \pm 0.12	840	
ECMWF	45°	Ascending	0.83 \pm 0.21	0.092	-0.07 \pm 0.12	1082
		Descending	0.82 \pm 0.25	0.069	-0.05 \pm 0.12	929
	52.5°	Ascending	0.84 \pm 0.17	0.088	-0.07 \pm 0.11	1161
		Descending	0.87 \pm 0.19	0.059	-0.04 \pm 0.11	883
	60°	Ascending	0.84 \pm 0.20	0.091	-0.07 \pm 0.11	1095
		Descending	0.85 \pm 0.25	0.059	-0.04 \pm 0.13	712
Mean	Ascending	0.86 \pm 0.18	0.090	-0.07 \pm 0.12	988	
	Descending	0.91 \pm 0.17	0.054	-0.04 \pm 0.13	671	

Several input parameters required for radiative transfer equation based soil moisture retrievals (e.g. Q , h , ω) were optimized for the OzNet sites in the Murrumbidgee catchment. The roughness parameter h and ω were found to be important parameters and showed dependency on the incidence angles when optimized against in situ soil moisture. When using LPRM for SMOS L-band observations, it would appear that ω is the most important parameter for its performance based on correlations. Better understanding of the behavior of ω may be an important step towards further improvement of the LPRM algorithm.

Two proposed methods to estimate effective temperature (De Rosnay & Wigneron, 2005; Holmes et al., 2012; Wigneron et al., 2001), using MERRA and ECMWF model outputs, were evaluated for LPRM and similar evaluation results were obtained. However, further research is needed to assess their performance in other regions or globally as systematic errors in T_{eff} may vary spatially (Parinussa et al., 2011b).

These results currently only apply to the OzNet sites but the evaluation results presented may serve as a baseline for further development of the LPRM model for L-band observations, with further focus on the ω , h and combining retrievals from different incidence angles towards a global soil moisture product.

Acknowledgments

This work was partially supported under the Water Information Research and Development Alliance between the Australian Bureau of Meteorology and CSIRO Water for a Healthy Country Flagship. I would like to thank CSIRO for their hospitality and for giving me the opportunity to conduct this research with their support. We would also like to thank the staff at the University of Melbourne and Jeff Walker and his colleagues at Monash University who have led the OzNet program. This project is partly funded by the ESA project "Passive Microwave Soil Moisture Data Fusion Study" (Contract # 4000110112). Further funding was provided by the European Space Agency Climate Change Initiative for soil moisture (<http://www.esa-soilmoisture-cci.org/>), contract no. 4000112226/14/I-NB.

Appendix A. Supplementary data

Supplementary data to this article can be found online at <http://dx.doi.org/10.1016/j.rse.2015.03.006>.

References

Balsamo, G., Viterbo, P., Beljaars, A., VandenHurk, B., Hirschi, M., Betts, A.K., et al. (2009). A revised hydrology for the ECMWF model: Verification from field site to terrestrial water storage and impact in the integrated forecast system. *Journal of Hydrometeorology*, 10(3). <http://dx.doi.org/10.1175/2008JHM1068.1>.

- Bisselink, B., Van Meijgaard, E., Dolman, A.J., & De Jeu, R.A.M. (2011). Initializing a regional climate model with satellite-derived soil moisture. *Journal of Geophysical Research-Atmospheres*, 116(D2). <http://dx.doi.org/10.1029/2010JD014534>.
- Bolten, J.D., Crow, W.T., Zhan, X., Jackson, T.J., & Reynolds, C.A. (2010). Evaluating the utility of remotely sensed soil moisture retrievals for operational agricultural drought monitoring. *IEEE Journal of Selected Topics in Applied Earth Observations and Remote Sensing*, 3(1). <http://dx.doi.org/10.1109/JSTARS.2009.2037163>.
- Brocca, L., Melone, F., Moramarco, T., Wagner, W., Naeimi, V., Bartalis, Z., et al. (2010). Improving runoff prediction through the assimilation of the ASCAT soil moisture product. *Hydrology and Earth System Sciences*, 14, 1881–1893. <http://dx.doi.org/10.5194/hess-14-1881-2010>.
- Camps, A., Vall-llossera, M., Corbella, I., Duffo, N., & Torres, F. (2008). Improved image reconstruction algorithms for aperture synthesis radiometers. *IEEE Transactions on Geoscience and Remote Sensing*, 46(1), 146–158.
- Choudhury, B., Schmugge, T., & Mo, T. (1982). A parameterization of effective soil temperature for microwave emission. *Journal of Geophysical Research*, 1301–1304.
- Crow, W., & Van den Berg, M. (2010). An improved approach for estimating observation and model error parameters for soil moisture data assimilation. *Water Resources Research*, 45(15). <http://dx.doi.org/10.1029/2010WR009402>.
- De Jeu (2003). *Retrieval of land surface parameters using passive microwave remote sensing*. (PhD dissertation) Amsterdam: VU University, 122.
- De Jeu, R.A.M., Dorigo, W.A., Parinussa, R.M., Wagner, W., & Chung, D. (2012). [Global climate] soil moisture. *State of the climate in 2011. Bull. Amer. Meteor. Soc.*, Vol. 93. (pp. 530–534). 7.
- De Jeu, R.A.M., Holmes, T.R.H., Panciera, R., & Walker, P. (2009). Parameterization of the land parameter retrieval model for L-band observations using the NAFE'05 data set. *IEEE Geoscience and Remote Sensing Letters*, 6(4). <http://dx.doi.org/10.1109/LGRS.2009.2019607>.
- De Jeu, R.A.M., Parinussa, R., Chung, D., Dorigo, W., Wagner, W., & Kidd, R. (2014). *Soil moisture retrieval from passive microwave sensors: Algorithm theoretical baseline document, version 2.0*. ESA CCI Soil Moisture, 30.
- De Lannoy, G.J.M., Reichle, R.H., & Pauwels, V.R.N. (2013). Global calibration of the GEOS-5 L-band microwave radiative transfer model over nonfrozen land using SMOS observations. *Journal of Hydrometeorology*, 14(3). <http://dx.doi.org/10.1175/JHM-D-12-092.1>.
- De Lannoy, G.J.M., Reichle, R.H., & Vrugt, J.A. (2014). Uncertainty quantification of GEOS-5 L-band radiative transfer model parameters using Bayesian inference and SMOS observations. *Remote Sensing of Environment*, 148, 146–157. <http://dx.doi.org/10.1016/j.rse.2014.03.030>.
- De Rosnay, P., & Wigneron, J. -P. (2005). Parameterizations of the effective temperature for L-band radiometry. Intercomparison and long-term validation with SMOSREX field experiment. In C. Mätzler (Ed.), Stevenage, UK: Institution of Electrical Engineers (ch 4.5).
- De Rosnay, P., Wigneron, J. -P., Holmes, T.R.H., & Calvet, J. -C. (2006). Parameterizations of the effective temperature for L-band radiometry. Inter-comparison and long term validation with SMOSREX field experiment. In C. Mätzler (Eds.), *Thermal microwave radiation: Application for remote sensing*. London, UK: IEE Electromagnetic Waves series, 52.
- Dorigo, W. A., Scipal, K., Parinussa, R. M., Liu, Y. Y., Wagner, W., De Jeu, R. A. M., et al. (2010). Error characterisation of global active and passive microwave soil moisture datasets. *Hydrology and Earth System Sciences*, 14, 2605–2616. <http://dx.doi.org/10.5194/hess-14-2605-2010>.
- Dumedah, G., Walker, J.P., & Rüdiger, C. (2014). Can SMOS data be used directly on the 15-km discrete global grid? *IEEE Transactions on Geoscience and Remote Sensing*, 52(5), 2538–2544. <http://dx.doi.org/10.1109/TGRS.2013.2262501>.
- Entekhabi, D., Njoku, E.G., O'Neill, P.E., Kellogg, K.H., Crow, W.T., Edelstein, W.N., et al. (2010). The soil moisture active passive (SMAP) mission. *Proceedings of the IEEE*, 98(5), 704–716. <http://dx.doi.org/10.1109/JPROC.2010.2043918>.
- Escorihuela, M.J., Kerr, Y.H., De Rosnay, P., Wigneron, J.P., Calvet, J.C., & Lemaitre, F. (2007). Simple model of the bare soil microwave emission at L-band. *IEEE Transactions on Geoscience and Remote Sensing*, 45(7), 1978–1987.
- Gruhier, C., De Rosnay, P., Hasenauer, S., Holmes, T.R.H., De Jeu, R.A.M., Kerr, Y., et al. (2010). Soil moisture active and passive microwave products: Intercomparison and evaluation over a Sahelian site. *Hydrology and Earth System Sciences*, 14, 141–156.
- Holmes, T.R.H., De Jeu, R.A.M., Owe, M., & Dolman, A.J. (2009). Land surface temperature from Ka band (37 GHz) passive microwave observations. *Journal of Geophysical Research-Atmospheres*, 114(D04), 113. <http://dx.doi.org/10.1029/2008JD010257>.
- Holmes, T.R.H., Jackson, T.J., Reichle, R.H., & Basara, J.B. (2012). An assessment of surface soil temperature products from numerical weather prediction models using ground-based measurements. *Water Resources Research*, 48, W02531. <http://dx.doi.org/10.1029/2011WR010538>.
- Huilin, G., Wood, E.F., Drusch, M., Crow, W., & Jackson, T.J. (2004). Using a microwave emission model to estimate soil moisture from ESTAR observations during SGP99. *Journal of Hydrometeorology*, 5, 49–63. [http://dx.doi.org/10.1175/1525-7541\(2004\)005<0049:UAMEMT>2.0.CO;2](http://dx.doi.org/10.1175/1525-7541(2004)005<0049:UAMEMT>2.0.CO;2).
- Jung, M., Reichstein, M., Ciais, P., Seneviratne, S., Sheffield, J., Goulden, M., et al. (2010). Recent decline in the global land evapotranspiration trend due to limited moisture supply. *Nature*, 467(7319), 951–954. <http://dx.doi.org/10.1038/nature09396>.
- Kerr, Y.H., Waldteufel, P., Richaume, P., Wigneron, J.P., Ferrazzoli, P., Mahmoodi, A., et al. (2012). The SMOS soil moisture retrieval algorithm. *IEEE Transactions on Geoscience and Remote Sensing*, 50(5). <http://dx.doi.org/10.1109/TGRS.2012.2184548>.
- Kerr, Y.H., Waldteufel, P., Wigneron, J.P., Delwart, S., Cabot, F., Boutin, J., et al. (2010). The SMOS mission: New tool for monitoring key elements of the global water cycle. *Proceedings of the IEEE*, 98(5). <http://dx.doi.org/10.1109/JPROC.2010.2043043>.
- Le Vine, D.M., Jacob, S.D., Dinnat, E.P., de Matthaes, P., & Abraham, S. (2007a). The influence of antenna pattern on Faraday rotation in remote sensing at L-band. *IEEE*

- Transactions on Geoscience and Remote Sensing*, 45(9), 2737–2746. <http://dx.doi.org/10.1109/TGRS.2007.898237>.
- Le Vine, D.M., Lagerloef, G.S.E., Colomb, F.R., Yueh, S.H., & Pellerano, F.A. (2007b). Aquarius: An instrument to monitor sea surface salinity from space. *IEEE Transactions on Geoscience and Remote Sensing*, 45(7), 2040–2050. <http://dx.doi.org/10.1109/TGRS.2007.898092>.
- Liu, Y.Y., De Jeu, R.A.M., McCabe, M.F., Evans, J.P., & Van Dijk, A.I.J.M. (2011). Global long-term passive microwave satellite-based retrievals of vegetation optical depth. *Geophysical Research Letters*, 38(18). <http://dx.doi.org/10.1029/2011GL048684>.
- Liu, Y.Y., De Jeu, R.A.M., Van Dijk, A.I.J.M., & Owe, M. (2007). TRMM-TMI satellite observed soil moisture and vegetation density (1998–2005) show strong connection with El Niño in eastern Australia. *Geophysical Research Letters*, 32(15). <http://dx.doi.org/10.1029/2007GL030311>.
- Liu, Y.Y., Dorigo, W.A., Parinussa, R.M., De Jeu, R.A.M., Wagner, W., McCabe, M.F., et al. (2012a). Trend-preserving blending of passive and active microwave soil moisture retrievals. *Remote Sensing of Environment*, 123, 280–297. <http://dx.doi.org/10.1016/j.rse.2012.03.014>.
- Liu, Y.Y., Van Dijk, A.I.J.M., McCabe, M.F., Evans, J.P., & De Jeu, R.A.M. (2012b). Global vegetation biomass change (1988–2008) and attribution to environmental and human drivers. *Global Ecology and Biogeography*, 22(6). <http://dx.doi.org/10.1111/geb.12024>.
- Meesters, A.G.C.A., De Jeu, R.A.M., & Owe, M. (2005). Analytical derivation of the vegetation optical depth from the microwave polarization difference index. *IEEE Transactions on Geoscience and Remote Sensing*, 2(2), 121–123.
- Mo, T., Clough, B.J., Schmugge, T.J., Wang, J.R., & Jackson, T.J. (1982). A model for microwave emission from vegetation-covered fields. *Journal of Geophysical Research*, 87(C13), 11229–11237.
- Njoku, E.G., & Entekhabi, D. (1996). Passive microwave remote sensing of soil moisture. *Journal of Hydrology*, 184(1/2), 101–129.
- Owe, M., De Jeu, R.A.M., & Holmes, T.R.H. (2008). Multi-sensor historical climatology of satellite-derived global land surface moisture. *Journal of Geophysical Research*, 113, F01002. <http://dx.doi.org/10.1029/2007JF000769>.
- Owe, M., De Jeu, R.A.M., & Walker, J.P. (2001). A methodology for surface soil moisture and vegetation optical depth retrieval using the microwave polarization index. *IEEE Transactions on Geoscience and Remote Sensing*, 39(8), 1643–1654.
- Panciera, R., Walker, J., Kalma, J.D., Kim, E.J., Saleh, K., & Wigneron, J.P. (2009). Evaluation of the SMOS L-MEB passive microwave soil moisture retrieval algorithm. *Remote Sensing of Environment*, 113(2), 435–444.
- Parinussa, R.M., Holmes, T.R.H., & De Jeu, R.A.M. (2011a). Soil moisture retrievals from the WindSat spaceborne polarimetric microwave radiometer. *IEEE Transactions on Geoscience and Remote Sensing*, 50(7). <http://dx.doi.org/10.1109/TGRS.2011.2174643>.
- Parinussa, R.M., Holmes, T.R.H., Yilmaz, M.T., & Crow, W.T. (2011b). The impact of land surface temperature on soil moisture anomaly detection from passive microwave observations. *Hydrology and Earth System Sciences*, 15, 3135–3151. <http://dx.doi.org/10.5194/hess-15-3135-2011>.
- Reichle, R.H. (2012). *The MERRA-land data product. GMAO Office note no. 3 (version 1.2)*. Greenbelt, MD, USA: NASA Goddard Space Flight Center, 38 (available from http://gmao.gsfc.nasa.gov/pubs/office_notes).
- Reichle, R.H., Koster, R.D., De Lannoy, G.J.M., Forman, B.A., Liu, Q., Mahanama, S.P.P., et al. (2011). Assessment and enhancement of the MERRA land surface hydrology estimates. *Journal of Climate*, 24, 6322–6338.
- Reynold, C.A., Jackson, T.J., & Rawls, W.J. (1999). Estimating available water content by linking the FAO soil map of the world with global soil profile database and pedotransfer functions. *Proceedings of the AGU 1999 Springs conference, Boston, MA*.
- Rienecker, M.M., Suarez, M.J., Gelaro, R., Todling, R., Bacmeister, J., Liu, E., et al. (2011). MERRA: NASA's modern-era retrospective analysis for research and applications. *Journal of Climate*, 24, 3624–3648. <http://dx.doi.org/10.1175/JCLI-D-11-00015.1>.
- Rossato, L., De Jeu, R.A.M., Alvala, R., & Souza, S. (2011). Evaluation of soil moisture from satellite observations over South America. *International Journal of Remote Sensing*. <http://dx.doi.org/10.1080/01431161.2010.532169>.
- Rudiger, C., Calvet, J.C., Gruhier, C., Holmes, T.R.H., De Jeu, T.R.H., & Wagner, W. (2009). An intercomparison of ERS-Scat, AMSR-E soil moisture observations with model simulations over France. *Journal of Hydrometeorology*, 10, 431–447. <http://dx.doi.org/10.1175/2008JHM997.1>.
- Sabater, J.M., Rosnay, P., & Balsamo, G. (2011). Sensitivity of L-band NWP forward modeling to soil roughness. *International Journal of Remote Sensing*, 32(19), 5607–5620. <http://dx.doi.org/10.1080/01431161.2010.507260>.
- Schneeberger, K., Schwank, M., Stamm, C., De Rosnay, P., Mätzler, C., & Föhler, H. (2004). Topsoil structure influencing soil water retrieval by microwave radiometry. *Vadose Zone Journal*, 3(4), 1169–1179.
- Smith, A.B., Walker, J.P., Western, A.W., Young, R.I., Ellett, K.M., Pipunic, R.C., et al. (2012). The Murrumbidgee soil moisture monitoring network data set. *Water Resources Research*, 48, W07701. <http://dx.doi.org/10.1029/2012WR011976>.
- Su, C.-H., Ryu, D., Young, R., Western, A.W., & Wagner, W. (2013). Inter-comparison of microwave satellite soil moisture retrievals over Australia. *Remote Sensing of Environment*, 134, 1–11. <http://dx.doi.org/10.1016/j.rse.2013.02.016>.
- Taylor, K.E. (2001). Summarizing multiple aspects of model performance in a single diagram. *Journal of Geophysical Research-Atmospheres*, 106(D7), 7183–7192.
- Taylor, C.M., De Jeu, R.A.M., Guichard, F., Harris, P.P., & Dorigo, W.A. (2012). Afternoon rain more likely over drier soils. *Nature*, 489, 423–426. <http://dx.doi.org/10.1038/nature11377>.
- Ulaby, F.T., Moore, R.K., & Fung, A.K. (1986). *Microwave remote sensing: Active and passive. From theory to applications, Vol. III*. Norwood, MA: Artech House.
- Van de Griend, A.A., & Wigneron, J.P. (2004). *On the measurement of microwave vegetation properties: Some guidelines for a protocol*.
- Van Wijk, W.R., & De Vries, D.A. (1963). *Periodic temperature variations on a homogeneous soil*. Physics of the Plant Environment. Amsterdam: North-Holland Publ. Co, 102–143.
- Wagner, W., Lemoine, G., & Rott, H. (1999). A method for estimating soil moisture from ERS scatterometer and soil data. *Remote Sensing of Environment*, 70, 191–207.
- Wagner, W., Naeimi, V., Scipal, K., De Jeu, R.A.M., & Martinez-Fernandez, J. (2007). Soil moisture from operational meteorological satellites. *Hydrogeology Journal*, 15. <http://dx.doi.org/10.1007/s10040-006-0104-6>.
- Wang, J.R., & Choudhury, B.J. (1981). Remote sensing of soil moisture over bare field at 1.4 GHz frequency. *Journal of Geophysical Research*, 86, 5277–5282.
- Wang, J.R., & Schmugge, T.J. (1980). An empirical model for the complex dielectric permittivity of soils as a function of water content. *IEEE Transactions on Geoscience and Remote Sensing*, 18, 288–295.
- Wigneron, J.P., Laguerre, L., & Kerr, Y.H. (2001). A simple parameterization of the L-band microwave emission from rough agricultural soils. *IEEE Transactions on Geoscience and Remote Sensing*, 39(8), 1697–1707.
- Wigneron, J.P., Parde, M., Waldteufel, P., Chanzy, A., Kerr, Y., Schmid, S., et al. (2004). Characterizing the dependence of vegetation model parameters on crop structure, incidence angle and polarization at L-band. *IEEE Transactions on Geoscience and Remote Sensing*, 42(2), 416–425.
- Ye, N., Walker, J.P., Rudiger, C., Ryu, D., & Gurney, R.J. (2011). The effect of urban cover fraction on the retrieval of space-borne surface soil moisture at L-band. *19th International Congress on Modelling and Simulation* (pp. 3398–3404).